

Corrosion of NiTi Wires with Cracked Oxide Layer

Jan Racek, Petr Šittner, Luděk Heller, Jan Pilch, Martin Petrevec, and Petr Sedlák

(Submitted November 22, 2013; in revised form January 24, 2014; published online March 1, 2014)

Corrosion behavior of superelastic NiTi shape memory alloy wires with cracked TiO₂ surface oxide layers was investigated by electrochemical corrosion tests (Electrochemical Impedance Spectroscopy, Open Circuit Potential, and Potentiodynamic Polarization) on wires bent into U-shapes of various bending radii. Cracks within the oxide on the surface of the bent wires were observed by FIB–SEM and TEM methods. The density and width of the surface oxide cracks dramatically increase with decreasing bending radius. The results of electrochemical experiments consistently show that corrosion properties of NiTi wires with cracked oxide layers (static load keeps the cracks opened) are inferior compared to the corrosion properties of the straight NiTi wires covered by virgin uncracked oxides. Out of the three methods employed, the Electrochemical Impedance Spectroscopy seems to be the most appropriate test for the electrochemical characterization of the cracked oxide layers, since the impedance curves (Nyquist plot) of differently bent NiTi wires can be associated with increasing state of the surface cracking and since the NiTi wires are exposed to similar conditions as the surfaces of NiTi implants in human body. On the other hand, the potentiodynamic polarization test accelerates the corrosion processes and provides clear evidence that the corrosion resistance of bent superelastic NiTi wires degrades with oxide cracking.

Keywords bending, electrochemical corrosion tests, martensitic transformation, shape memory alloy, superelastic NiTi wires

1. Introduction

Improving fatigue lifetime and corrosion performance of NiTi stents has always belonged among the key issues of NiTi superelastic technologies for medical devices. This work was carried out as a part of a broader research program focused on the investigation of corrosion fatigue of braided NiTi stents in biological fluids (Ref 1, 2).

It is well known that the thickness and quality of the TiO₂ oxide layer on the surface of heat-treated NiTi wires crucially affects its corrosion behavior. Thin smooth oxide layers exhibit better corrosion resistance measured by electrochemical methods; nevertheless, even these are susceptible to pitting corrosion (Ref 3). Breakdown potentials of passive layer on the heat-treated NiTi wire after bending in martensite vary depending on the oxide thickness (Ref 4). The occurrence of the martensitic phase in strained wires results in the decrease of the corrosion potential, thus reducing the corrosion resistance of the austenitic NiTi (Ref 5). Degradation of corrosion properties of

superelastic NiTi with mechanical deformation thus seems to be confirmed. However, it is not clear yet whether this is due to the presence of the stress-induced martensite phase and stress in the material surface; or due to the cracking of the surface oxide of the strained wires.

Recently, effect of inclusions on fatigue and corrosion resistance of NiTi has been focused in the literature (Ref 6). Though we are aware of the occurrence of oxide and carbide inclusions in the wires we used, this was not dealt with in this paper. Neither was the goal to improve the corrosion performance. The sole purpose of this work was to characterize corrosion behavior of superelastic NiTi wires with cracked surface oxide layers, particularly to find out whether and how the oxide cracking affects the corrosion performance of NiTi and to identify appropriate methods for electrochemical characterization of NiTi wires with cracked oxide layers. Different states of surface oxide cracking were achieved by bending NiTi wires over four different diameters, cracks were observed by SEM/FIB technique; and electrochemical experiments on bent wires were performed to evaluate the effect of the degree of the surface oxide cracking on the corrosion behavior.

2. Material and Methods

2.1 Material and Samples for Electrochemical Experiments

Superelastic NiTi wire FWM#1 of 0.2 mm diameter, nominal chemical composition of ~50.8 at.% Ni (balance Ti), straight annealed with etched and mechanical polished surface was used to prepare samples. The wire was given the same heat treatment (510 °C for 3 min in fluid furnace in Al₂O₃, air atmosphere followed by cooling to room temperature in H₂O and washing in ethanol) in a straight shape. The same wire and heat treatment was used in the related work (Ref 2) to shape set NiTi springs for fatigue testing.

This article is an invited paper selected from presentations at the International Conference on Shape Memory and Superelastic Technologies 2013, held May 20–24, 2013, in Prague, Czech Republic, and has been expanded from the original presentation.

Jan Racek, Petr Šittner, Luděk Heller, and Jan Pilch, Department of Functional materials, Institute of Physics of the AS CR, v.v.i., Prague, Czech Republic; Martin Petrevec, TESCAN, Brno-Kohoutovice, Czech Republic; and Petr Sedlák, Institute of Thermomechanics, Prague, Czech Republic. Contact e-mail: racek@fzu.cz.

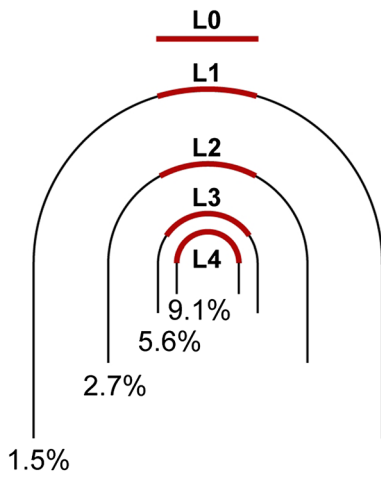


Fig. 1 Wire samples with different bending radii and equal uncovered arc lengths for electrochemical experiments. Various bending radii correspond to different surface strains and hence different states of the surface oxide cracking

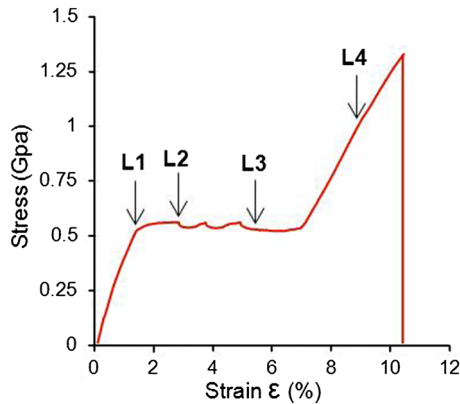


Fig. 2 The surface tensile strains on samples L1–L4 correspond to denoted states on the tensile σ – ε curve

Four types of U-bent wire samples were prepared by bending the heat-treated wire over mandrels of different radii L1–L4 (Fig. 1) and keeping them in the bent shape using special holder. The bent state can be characterized by the ratio $\varepsilon = r_w/R_b \times 100$ [%], (r_w and R_b are radius and bending radius of the wire, respectively) indicating mean value of maximal tensile and compressive (the absolute value) strains on the wire surface. Considering low value of ε , bending of the wire leads to linear strain distribution through the cross section of the wire, but the neutral (zero) strain axis deviates from the wire centerline due to tension-compression asymmetry (Fig. 3). Based on numerical simulation (Ref 7, the ratio of transformation strain in tension to transformation strain in compression was set as 1.5) the maximal tensile strains 1.5, 2.6, 5.6, and 9.1 % (Fig. 2) and thicknesses of the partial transformed surface layers (vol. fraction of martensite > 10 %) for L1–L4 samples (Fig. 4) were evaluated.

2.2 SEM/EDX/FIB and TEM Observations

SEM/EDX and TEM techniques were employed to characterize the wire surface. The surface oxide and microcracks in it

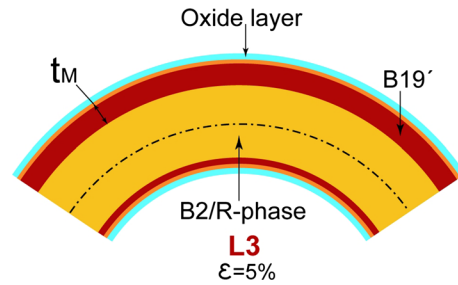


Fig. 3 Schematic picture of phase composition in bended wire (lateral cut) with thickness t_M of the transformed B'19 layer of the bent wire

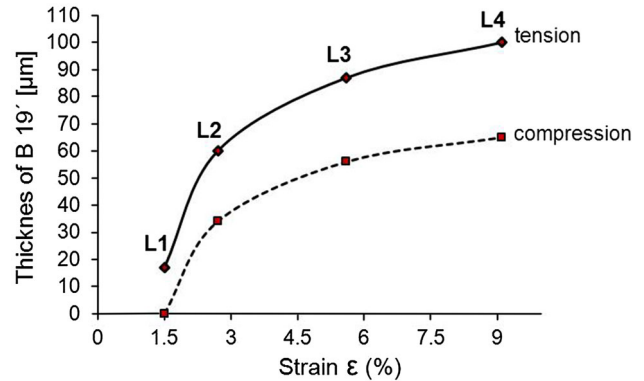


Fig. 4 Thickness of B'19 layer increasing with decreasing bending radius

were observed by SEM using the top view as well as on cross sections prepared using the FIB technique. EDX spectra provided information about the chemical composition within various surface and subsurface layers. TEM observations on FIB cross section lamella were performed to characterize the surface oxide layer and subsurface NiTi matrix layer in more detail. The SEM/FIB observations and TEM lamella preparation were performed using the MIRA and LYRA TESCAN instruments combining SEM/EDX with FIB—a Ga^+ ion beam etching column. The TEM observations were performed in a Philips CM12 TEM/STEM with acceleration voltage 120 kV.

2.3 XPS Surface Analysis and Depth Profile Characterization

XPS depth profile analysis was carried out on gradually sputtered surface to evaluate concentration gradients from the surface oxide layer down to NiTi matrix. Analysis was performed with a ESCA⁺ Omicron. The UHV system pressure in analyzer chamber was maintained near 10^{-11} mbar. Spectra were obtained using a monochromatic Al K α (1486.6 eV) x-ray source. All binding energies were referenced to the graphitic carbon C1s peak at 284.7 eV. The XPS input data were compiled and analyzed using CasaXPS software. Ar ion sputtering at 5 keV by step of 5–30 min was employed for estimation of depth profile up to 160 nm. Sputtering 10 min of Ar ions corresponded to 13–15 nm. Correlation of sputtering time versus depth was first calibrated by sputtering Ti sheet and measuring the groove by profilometer. The thickness of the

concentration profile through the oxide layer corresponds well to the oxide thickness measured by SEM.

2.4 Electrochemical Tests

The electrochemical studies were performed in a 0.9 % NaCl solution at temperature 37 °C using a GAMRY potentiostat. A few drops of dilute HCl were used to adjust the pH = 3. According to Pourbaix diagram, TiO₂ is stable in the whole range of stability of water and TiO₂ is passive and resistant to chlorides at pH = 3 (Ref 12). Reference 600 potentiostat was used in three-electrode configuration (working electrode, counter graphite, and reference SCE electrodes) as shown in Fig. 5. The solution was purged with argon for 1 h prior to testing, and purging continued also during the measurements. The sample surfaces were covered by a lacquer except of the arc 3.93 mm long in locations of constant bending radius, so that the surface areas exposed to electrolyte were equal (see Fig. 1). The open circuit potential (OCP) measurements were carried out to characterize basic electrochemical characteristics of the samples L0, L1, and L4 before electrochemical impedance spectroscopy (EIS) and potentiodynamic polarization (PP) tests. OCP measurement was performed for 120 min just prior EIS. EIS experimental setup featured 5 mV amplitude, freq. range 100 kHz to 1 MHz, and sample area 0.025 cm². Low impedance of reference electrode was accomplished by setting proper distance from the working electrode and using large surface area of the counter platinum electrode. The Potentiodynamic Polarization was performed using scan rate of 0.1 mV/s beginning from -700 mV to potential above 1.2 V.

3. Characterization of the Surfaces of the Straight and Bent NiTi Wires

3.1 Characterization of the Surface Oxide on the Straight NiTi Wire

The oxide layer on the NiTi straight wire surface was characterized by FIB-SEM/EDX. Various FIB cross sections

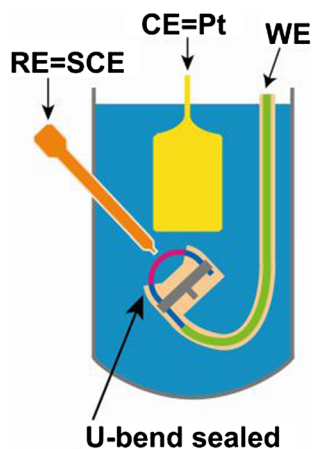


Fig. 5 Three electrodes arrangement in the electrochemical cell where RE is reference saturated calomel electrode with very close distance from WE working electrode of sealed U-bend sample, CE is counter platinum electrode

were prepared by FIB technique to investigate the thickness and morphology of the surface oxide layer (Fig. 6, 7). Platinum (GIS) was injected on the surface before FIB cutting to preserve the wire surface. It can be seen on the perpendicular cut (Fig. 6b) that surface oxide layer of constant thickness (≈ 70 nm) closely follows the roughness of the NiTi surface. Additionally, a thin lamella ($t < 100$ nm) was prepared by FIB cutting and polishing roughly parallel to the wire surface with the aim to evaluate the surface oxide morphology and perform its chemical analysis by EDX (Fig. 7). In this way, it was possible to follow the inhomogeneous morphology of the oxide layer by STEM technique (if there were oxide cracks, they were introduced during the lamella preparation). Compositional variations measured by EDX were used to determine the regions of Pt, Oxide, and NiTi matrix. A nickel-rich layer (Ref 8) which was expected to exist underneath of TiO₂ oxide layer in the NiTi matrix could not be reliably detected by this way. Ni-enrichment is due to the selective oxidation, titanium has a higher affinity for oxygen than nickel. Free enthalpy of NiO, TiO, and TiO₂ formation ΔG (298K) is -211.7, -495, and -889.5 kJ mol⁻¹.

3.2 Characterization of the Surface Oxide on the Bent NiTi Wire

Microscopic SEM observations of the surface oxide cracks were carried out on the tensile side of the bent wire samples L1-L4 prior to electrochemical experiments (Fig. 8). Utmost care was taken to assure that the cracks were indeed created by bending (wires were carefully shape set in straight form and

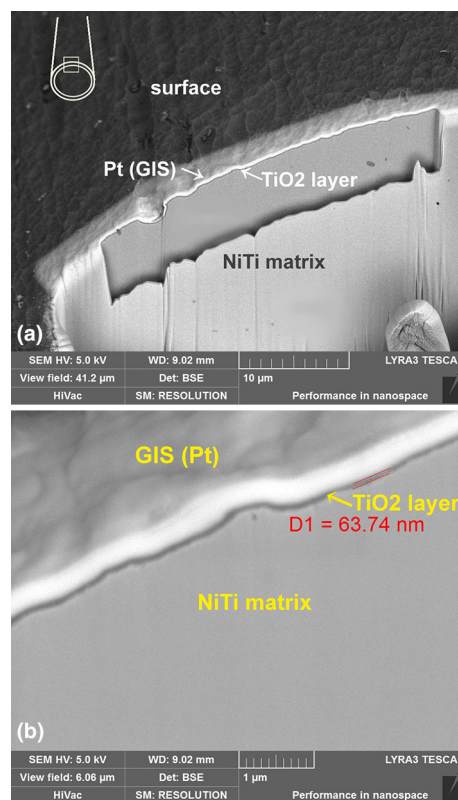


Fig. 6 SEM/FIB characterization of the wire surface: (a) edge view of the FIB section perpendicular to the wire surface, (b) detail—thickness of the surface oxide layer measured on the FIB section

bent only once over the mandrel). We already had experience with the observation of surface oxide cracking in situ during straining the superelastic wires in SEM—see related paper (Ref 2). Isolated oxide cracks were found already on the surface of the sample L1 having surface strain 1.5 % (Fig. 1, 2) and martensitic layer underneath the oxide (Fig. 3, 4). It can be clearly seen (Fig. 8) that the density of cracks (number and mutual separation) and crack opening widths increase with increasing bending radius (surface strain). It comes out that the bent NiTi wires (samples L1–L4) are covered by cracked oxide

layers with density and widths of cracks increasing with decreasing bending radius. This information was used to inform the models used to interpret the results of electrochemical parameters.

3.3 Microcracks Observed on FIB Cross Sections from the Bent NiTi Wire

Microcracks in the cracked surface oxide layer were also studied on perpendicular FIB cross sections prepared from the

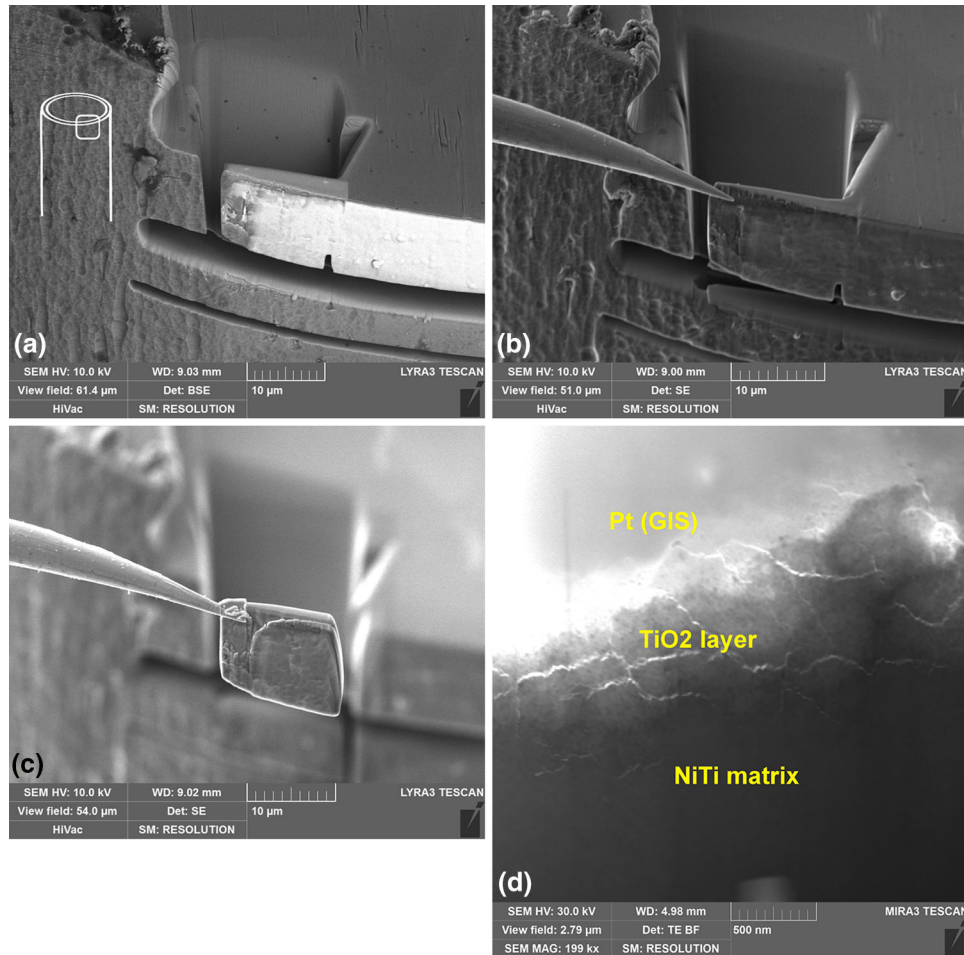


Fig. 7 Lamella (100 nm) manufactured parallel to the wire surface by FIB cutting and polishing: (a) FIB cutting by Ga ions at the wire surface covered GIS layer, (b) Lamella approached by a needle after polishing and before final cut, (c) lamella removed by the needle, (d) STEM observation of the morphology of the oxide layer on the lamella (width of the inclined oxide layer was determined ~500 nm by EDX analysis)

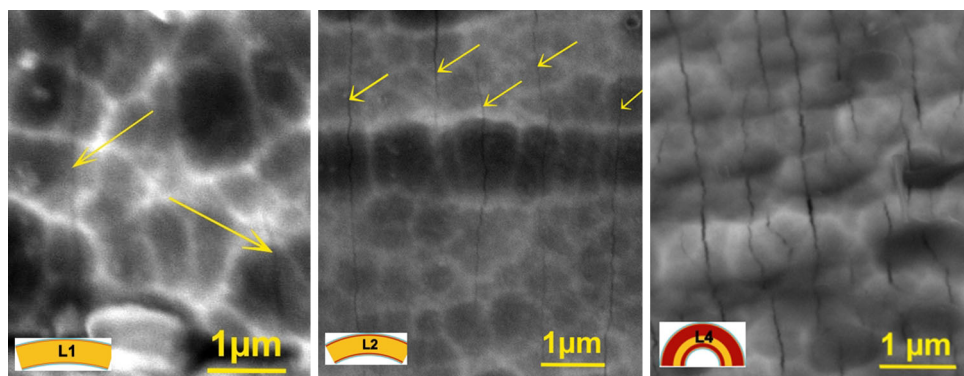


Fig. 8 SEM images of the surfaces of the bent NiTi wire samples L1 = 1.4 %, L2 = 2.5 %, and L4 = 8 %

maximally bent wire L4 by SEM and TEM methods. Of course the cracks are allowed to close in this case and there is a danger that additional crack could be introduced during FIBing. Figure 9 shows SEM picture of the edge of the FIB lamella, where the oxide cracks can be seen both on the wire surface as well as on the polished cross section. The matrix cracks are short (<200 nm); the long vertical traces are polishing artefacts. Mutual one to one correspondence, however, suggests that the surface oxide cracks do extend into the NiTi matrix.

Microcracks in the surface oxide layer were also found by the TEM observation on another perpendicular FIB lamella from the maximally bent wire L4 (Fig. 10). Thickness of the oxide layer was found to be around 80 nm similar to the SEM results and its morphology was inhomogeneous. Nanosized grains of the partially recrystallized microstructure of the NiTi wire within the matrix are clearly visible. The crack shown in Fig. 10 penetrates only few nm into the NiTi matrix. Dislocation defects were frequently observed in the NiTi matrix in the vicinity of surface oxide cracks. However, since these are very preliminary observations made on a single lamella prepared from just once superelastically bent NiTi wire L4, the conclusion which is made is that the surface oxide cracks introduced by bending do penetrate into the NiTi matrix of the superelastically bent wire. The cracks crossing over into the matrix are further considered as a kind of gates (density and width increasing with decreasing bending radius) through which the electrolyte may reach the NiTi matrix in the electrochemical experiments.

3.4 Chemical Composition Profile Through the Wire Surface

Information on chemical composition of the NiTi wire surface was obtained by XPS surface and depth profile analysis. Ar ion sputtering was used to evaluate chemical composition up to 160 nm. One of the objectives was to identify the Ni-rich layer underneath of TiO₂. Since the NiTi wire is too thin, multiple wires were laid down in parallel for the measurement. Results are shown in Fig. 11a. It is rather difficult to identify the exact boundary between the oxide and matrix from the measured XPS profile. This was ascribed to the cylindrical surface of the thin wires with irregularities. Therefore, a comparative analysis was carried out on a flat surface of a polished disk cut from 1.9-mm-thick wire of the same material. The disk was heat treated (oxidized) by the same heat

treatment. It was assumed that the thickness and quality of the surface oxide approximately correspond to that of the original thin wire used for the stent production. The XPS results from the thin wires and polished disc presented in Fig 11a,b indeed show similar concentration profiles. The width of the oxide layer of about 70 nm is estimated. There seems to be a Ni-rich layer of about 20 nm in the matrix underneath the interface but the evidence is not very convincing. The increase of Ni at the outmost layer of the surface oxide (Fig. 11a,b) was associated with the NiO distinguished in Ni 2p_{3/2} spectrum. Although the presence of the Ni excess at the very surface is known from the literature (Ref 8, 9), its consequences for corrosion are not very clear, so we are not considering it here. For comparison, Fig. 11c shows XPS depth profile from the disc of the same material, which was mechanically polished but not heat treated. Clearly, the surface oxide layer is only few nm thick in this case. Since relatively high content of oxygen 3–5 wt.% was detected deep in the NiTi matrix even in the sample which was not heat treated; the presence of oxygen in the NiTi matrix is considered to be an artefact, although the NiTi matrix is known to contain oxide particles (Ref 10).

4. Electrochemical Studies

Three electrochemical methods (Open Circuit Potential, Electrochemical Impedance Spectroscopy, and Potentiodynamic Polarization) were employed successively to evaluate to corrosion resistance of straight L0 and bent superelastic NiTi wire samples L1–L4 in simulated biological fluid (0.9 % solution of NaCl, pH = 3) at temperature 37 °C. Three measurements were performed in each experimental set to assure that the targeted effect of cracked oxide and increasing bending strain on the corrosion behavior of NiTi is significant and reproducible.

4.1 Corrosion Activity of the Surface (Open Circuit Potential)

The results of the OCP measurements (Fig. 12) provide basic electrochemical information on samples L0–L4 in a form of the time evolution of the corrosion potential (Ref 11). In general, the higher is the value of the corrosion potential at the

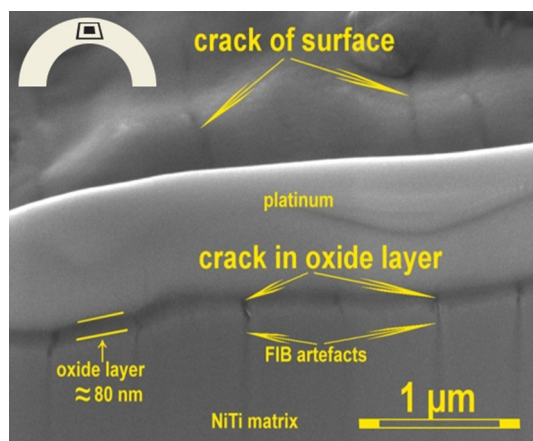


Fig. 9 Microcracks in the TiO₂ surface oxide observed by SEM on the edge of FIB cross section prepared from the L4 sample

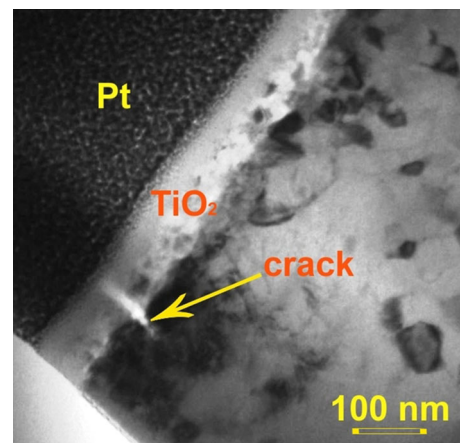


Fig. 10 TiO₂ surface oxide observed by TEM (FIB lamella prepared from the L4 sample)

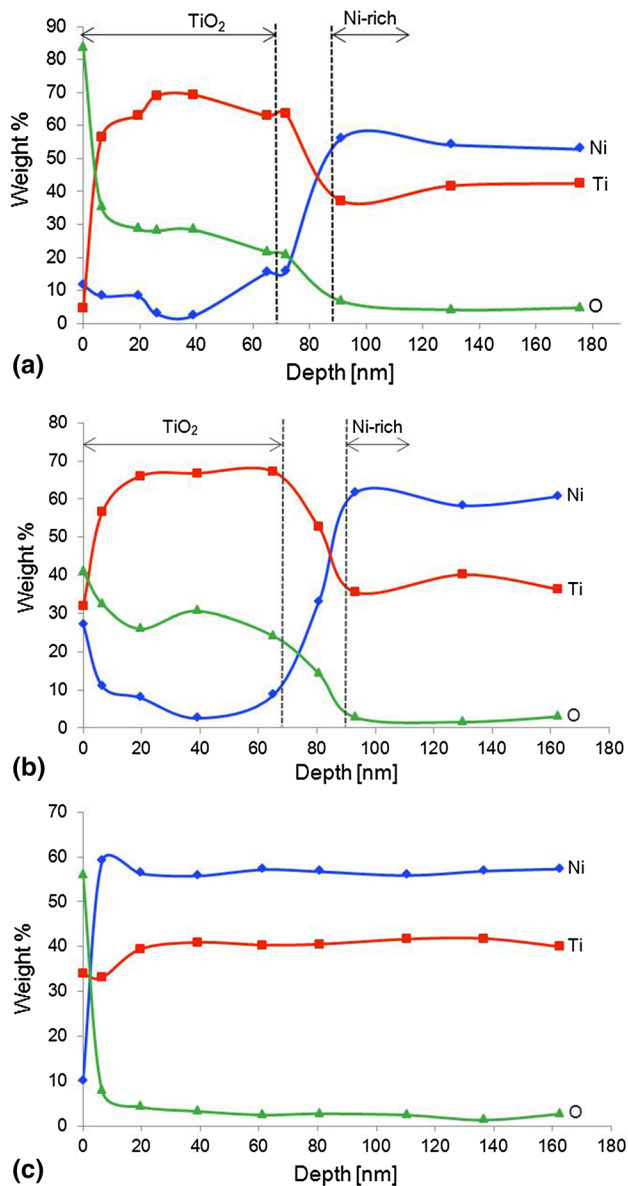


Fig. 11 (a) XPS depth profile from thin NiTi wire (multiple 0.2 mm thin wires laid down in parallel). Two distinct layers were identified in addition to NiTi matrix: TiO₂ layer and Ni-rich layer in the NiTi matrix. (b) XPS depth profile from flat surface of a cylinder cut from 1.9-mm-thick wire of the same alloy, polished and given similar heat treatment as the wires. Two distinct layers were identified: TiO₂ oxide layer and Ni-rich layer in NiTi matrix. NiO concentration increased on top of surface oxide layer. (c) XPS depth profile of the as-drawn NiTi #1 ($d = 1.8$ mm wire cross section), mechanically polished, and no heat treatment

end of test, the higher is the corrosion resistance of the studied sample. Therefore, sample L0 may be considered as more corrosion resistant and more thermodynamically stable compared to bent wire samples, since its corrosion potential becomes significantly higher from 30 min up. This suggests that the bent NiTi wires with strained surface and cracked oxide are more prone to corrosion degradation than the straight wire (Table 1). It was, however, not possible to make a meaningful conclusion on the role of the increasing surface strain

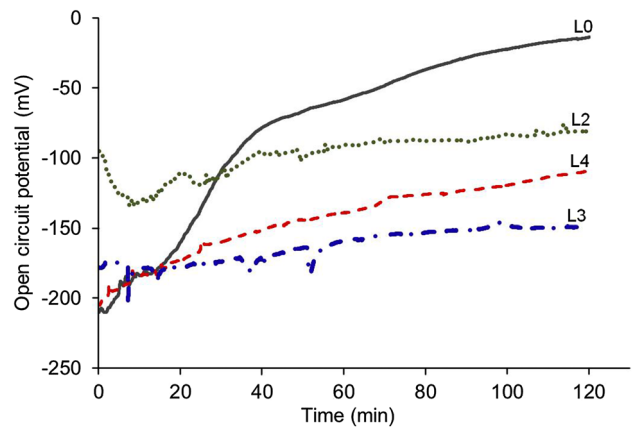


Fig. 12 Results of the Open Circuit Potential measurement characterizing corrosion activity of samples L0, L2, L3, and L4 in 0.9 % NaCl solution, pH 3

(decreasing bending radius) of the samples L2–L4 based on the individual OCP curves.

4.2 Passivity Breakdown (Potentiodynamic Polarization)

The potentiodynamic polarization test basically characterizes the passivity of the sample surface (chemical stability in a given environment characterized by pH for varying electrical potential. The results are quantified mainly by the breakdown potential E_b and corrosion current I_{corr} . The PP test represents a standard electrochemical test for characterization of the corrosion behavior of NiTi. It has been widely applied in the literature (Ref 12) to characterize the corrosion performance of NiTi wires having various surface finishing treatments. We show only results of measurements on samples L0, L3, and L4 in Fig. 13 for the sake of clarity. The straight wire sample L0 clearly exhibits more stable electrochemical response (the highest breakdown potential E_b and the lowest corrosion current I_{corr}) compared to the bent wire samples L3 and L4 with cracked oxide layers. As a result of the bending, the corrosion current I_{corr} of the NiTi wire increased from 7 pA/cm² (L0) to 194 pA/cm² (L3), breakdown potential E_b decreased from 670 mV (L0) down to 430 mV (L4), corrosion potential E_{corr} decreased, and corrosion rate significantly increased (Table 1). This proves significant degradation of the corrosion properties of the NiTi wire due to bending. It is, however, again difficult to make a meaningful conclusion on the effect of the degree of bending on potentiodynamic polarization curves. It has been concluded that the virgin oxide layer on the straight NiTi wire provides a relatively good protection against corrosion in acidic environment with chlorides. The corrosion resistance, however, significantly decreases when the surface oxide is strained; cracks appear in it and are kept open by the applied constraint.

4.3 Equivalent Circuit for Cracked Oxide Layer (Electrochemical Impedance Spectroscopy)

Electrochemical Impedance Spectroscopy measurement is a relatively modern electrochemical test, which has not been used much in the literature to characterize corrosion properties of NiTi. The results are shown in a form of Nyquist plot (Fig. 14a) and Bode plot (Fig. 14b) showing impedance and phase shift,

Table 1 Results of OCP and PP Measurements on Samples L0 (Straight Wire) and L2, L3, and L4 (Bent Wires)

Sample	OCP		Potentiodynamic polarization			
	E_{corr} vs SCE (mV)	I_{corr} ($\mu\text{A}/\text{cm}^2$)	E_{corr} (mV)	E_b (mV)	I_b (nA)	Corr. rate (mpy)
L0	-14	7	-94	670	0.5	133.5e-9
L2	-109
L3	-149	194	-256	500	8.3	4.5e-6
L4	-109	100	-196	430	4.1	2.3e-6

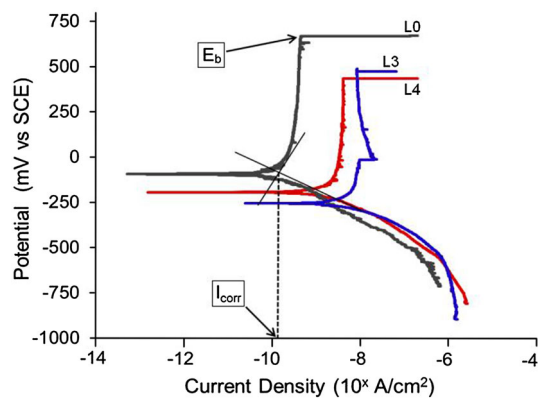


Fig. 13 Results of the potentiodynamic polarization test on samples L0, L3, and L4. Higher value of the breakdown potential E_b and lower value of the corrosion current I_{corr} suggest increased passivity of the surface oxide and better corrosion properties

respectively, evaluated using small AC voltage applied in a wide frequency range. Interpretation of the EIS experimental data is standardly achieved via modeling using the so-called electrical equivalent circuit consisting of electrical components representing physical parameters of the studied sample surface. Parameters of such circuits are identified by fitting the simulated data to the experimental ones. An equivalent circuit must be properly designed to correlate with the corrosion properties of the studied corrosion system.

Equivalent circuit $R_s(Q_1(W(Q_2R_c)(Q_3R_p)))$ for bent NiTi wires (Fig. 15) comprise the following elements: electrolyte resistance R_s , non-ideal capacitance of double layer Q_1 (C_{dl}), Warburg diffusion capacitance W , non-ideal capacitance of crack Q_2 (C_c), resistance of crack R_c , non-ideal capacitance of oxide layer Q_3 (C_o), and polarization resistance R_p . The infinite Warburg diffusion capacitance was added in series with the resistance of crack R_c to indicate dependencies of ionic charge transfer on increased concentration gradient of corrosion reactants and products in the volume of crack. W diffusion is often observed in porous and defective layers susceptible to corrosion. The weakness of the model is that the state of the surface oxide on the bent NiTi wire is very far from homogeneous. Straight wire—virgin L0 sample was fitted using equivalent circuit $R_s(QR_p)$. There exist similar models for NiTi in the literature (Ref 22).

A simplex method algorithm (Ref 13, 14) was used for fitting the experimental data set to an equivalent circuit model (Fig. 15). The quality of data fit (Fig. 14) suggests that the proposed models show good match for all L0, L2, L3, and L4 samples. The obtained values of the individual components of electrical equivalent circuit for samples L0, L2, L3, and L4 are

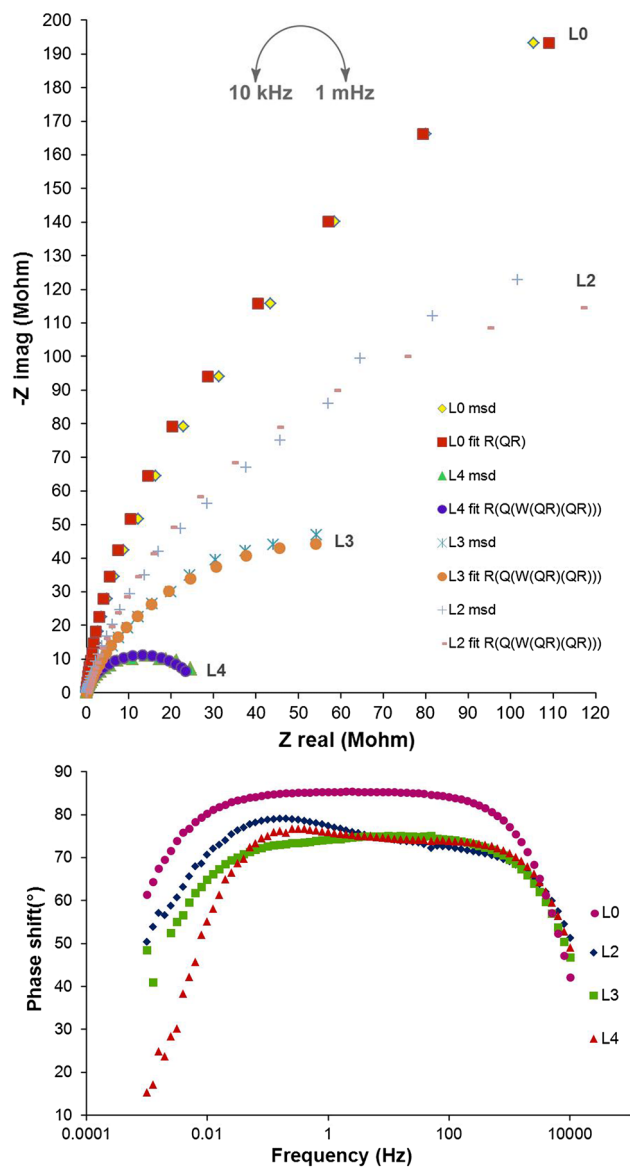


Fig. 14 (a) Nyquist plot impedance curves of samples L0, L2, L3, and L4 measured in Electrochemical Impedance Spectroscopy test 5 mV amplitude, freq. range 100 kHz to 1 mHz). Measured values are compared with values obtained by fitting the equivalent circuit model of virgin and cracked oxide layers. (b) Bode plot evaluated from the same measurement as in 14a. The sample L0 represents ideal and smooth virgin surface while samples L2, L3, and L4 have heterogeneous cracked surface. The phase shift is highest for the L0 at any frequency and the curves L2, L3, and L4 are affected by the surface state mainly in the low frequency range where the impedance is dominated by the capacity of heterogeneous cracked layer

summarized in Table 2. The employed equivalent circuits for impedance spectra analysis in the model do have a physical meaning (Fig 17). It is evident that the polarization resistance R_p (magnitude of polarization vector) drastically and consistently decreases with increasing surface strain (Fig. 16). Decreasing value of the empirical constant n of the constant phase element (non-ideal capacitor) from L2 to L4 (related to the electrode roughness and heterogeneities) suggests that surface roughness of the bent wire increases with decreasing radius.

5. Discussion

As compared to electrochemical studies on stress-free superelastic NiTi published frequently in the literature (mostly potentiodynamic polarization tests), three key factors which make the present experiments on bent superelastic NiTi wires unique are following: (i) the surface in contact with the electrolyte is exposed to mechanical stress, (ii) the surface oxide of the bent wire is fractured, and (iii) the cracks are kept open during the electrochemical experiment. The distribution of static stresses in the surface layer along the circumference of the U bend sample changes from tensile to compressive. Stress-induced martensite and surface oxide cracking preferentially appears in locations where maximal tensile stress component is

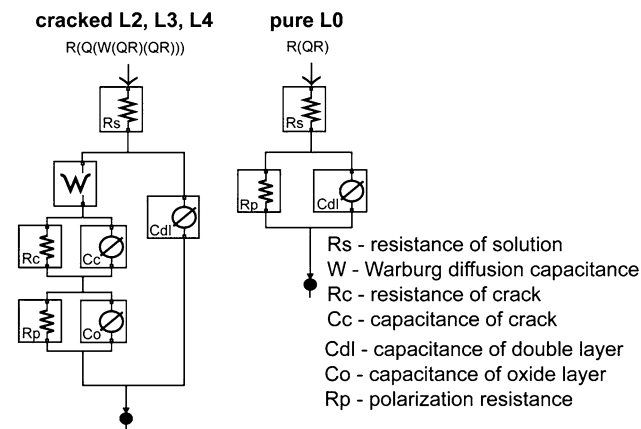


Fig. 15 Proposed equivalent circuit model for cracked and virgin oxide layer on NiTi bent wire

reached (Ref 2). Although Fig. 3 and 17 assume a continuous martensite layer existing under the surface oxide, this is a simplification suggesting only that the martensite preferentially appears at the upper surface of the bent wire. In reality, mixture of all three phases in NiTi (B2, B19', and R-phase) exist in the matrix under the oxide layer (Ref 15) and the martensite does not have to be distributed homogeneously along the arc. The electrolyte is thus probably in contact not only with the austenite but also with the stress-induced martensite and

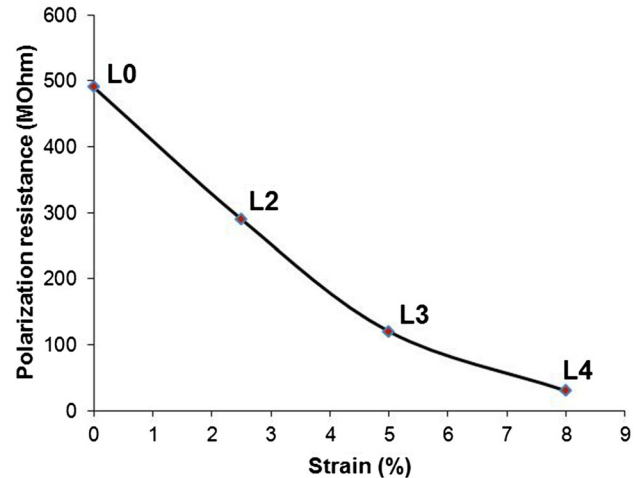


Fig. 16 Polarization resistance R_p evaluated from the EIS experiment decreases with increasing surface strain (bending radius) of samples L0, L2, L3, and L4

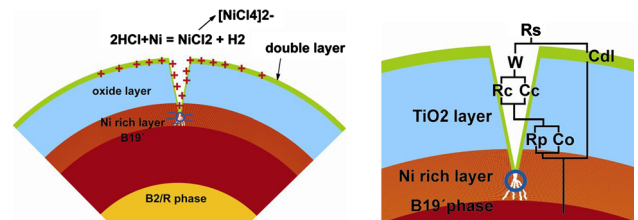


Fig. 17 Model of crack in oxide layer with anodic crack tip dissolution in oxide-martensite interface. Ni^{2+} ions are depleted from the crack tip by catalytic reaction of Cl^- ions (left). Physical meaning of the equivalent circuit proposed for cracked oxide layer (right)

Table 2 Parameters Fitted Using Proposed Equivalent Electrical Circuits for Samples L0 (Straight Wire) and L2, L3, and L4 (Bent Wires)

Sample	Equivalent circuit	R_s (Ω)	C_{dl} (Q) ($S \times s^{n_1}$)	n_1	$W S \times s^{1/2}$	C_c (Q) ($S \times s^{n_2}$)	n_2	R_c (Ω)	C_o (Q) $S \times s^{n_3}$	n_3	R_p (Ω)	χ^2
L0	R(QR)	63	4.8E-7	0.94	4.9E8	0.00093
L2	R(Q(W(QR)(QR)))	152	2.2E-7	0.87	1.6E-6	2.9E-7	0.9	7.6E7	3.2E-7	0.86	2.9E8	0.00015
L3	R(Q(W(QR)(QR)))	129	3.7E-7	0.80	4.3E-6	6.8E-6	0.85	...	1.3E-7	0.89	1.2E8	0.00125
L4	R(Q(W(QR)(QR)))	54	7.2E-7	0.87	1582	1.3E-6	0.57	4.3E5	3.1E-7	0.96	2.6E7	0.00126

The meaning of the individual parameters is as follows: R_s is the electrolyte resistance, C_{dl} is the non-ideal capacitance of the double layer, n_1 is the coefficient of CPE = $1/Z = Y = Q^\circ (j\omega)^{n_1}$, where Q° has the numerical value of the admittance ($1/|Z|$) at $\omega = 1$ rad/s. The unit of Q° is Siemens-secondⁿ ($S s^n$), W is the Warburg infinite diffusion of crack defects, C_c is the non-ideal capacitance of crack, n_2 is the coefficient of CPE (C_c), R_c is the resistance of cracks containing corrosion products, C_o is the non-ideal capacitance of passive oxide, n_3 is the coefficient of CPE (C_o), and R_p is the polarization resistance of protective passive layer

R-phase. The stressed mixture of phases is considered to represent a “more open structure” compared to only B2 austenite phase (characteristic for conventional experiments in the literature Ref 3), particularly since it contains large number of internal interfaces. Hence, it is more susceptible to hydrogen diffusion from the electrolyte into the matrix and might facilitate hydrogen embrittlement, local and intercrystalline corrosion (Ref 16, 17).

Since the Open Circuit Potential test (Fig. 12) showed higher corrosion potential value for the straight wire compared to the bent wires, we conclude that corrosion activity of the cracked surface increases due to the above-mentioned three factors i–iii, mainly due to the presence of cracks in the oxide layer (Fig. 8) extending into the NiTi matrix. However, since the corrosion potential values of three bent wire samples L1, L2, and L3 scattered without any consistency, the OCP test was found not to be really appropriate for estimation of the effect of the decreasing bending radius.

Potentiodynamic polarization test (Fig. 13) showed lower E_b and higher I_{corr} values for all bent wire samples compared to the straight wire sample L0 which suggests that cracking of the oxide layer significantly deteriorates the surface passivity. Since the bent wire samples exhibit breakdown potentials on potentiodynamic curves, we assume that the wires are able to partially repassivate their surfaces damaged by the cracking. Since the NiTi wire surface is exposed to tensile and/or compressive stress and the oxide cracks are kept open by bending, the repassivation of the cracked oxide layer might be significantly limited by the stress and/or martensite phase at the crack tip. At the same time, number of cracks which penetrate into the subsurface Ni-rich layer increases with increasing bending strain which facilitates the penetration of electrolyte to the NiTi matrix and further complicates repassivation. Since Nickel does not react with oxygen to form passive surface oxide but reacts instead with chloride anions through catalytic reaction; the dissolution and crack advance should accelerate, if there is Ni-rich layer underneath the surface oxide layer. However, since no clear relation between the degree of the surface cracking and breakdown potentials of bent wires was found in present experiments, we speculate that the key factor influencing the passivation of bent NiTi wires is the presence of cracks in the oxide layer kept open by bending, not their density and width.

The key observation is that, contrary to other tests, there is a clear distinction among the Electrochemical Impedance Spectroscopy curves of the samples L0, L2, L3, and L4 differing in the extent of the surface oxide cracking in the Nyquist plot (Fig. 14a). This suggests that the method is sensitive to the state of the surface of the variously bent wires. Similar claims can be found in the electrochemical literature for other materials as well (Ref 18, 19). Recall that surfaces of differently bent NiTi wires differ in surface strain, stress, phase fraction and crack density and widths; and the analysis of the EIS results is not simple. Equivalent circuit model (Fig. 15) allows for identification of the evolution of physical parameters of cracked oxide layers with increasing surface damage through fitting the model to experimental results (Fig. 14a). Five parameters of the electrical circuit: (polarization resistance R_p , Warburg capacitance W , resistance of crack R_c , capacitance of oxide layer C_o , and capacitance of crack C_c) were found to vary consistently with decreasing bending radius (Table 2). Particularly, the polarization resistance R_p decreasing with increasing surface strain (Fig. 16) suggests that the increasing width and density of surface cracks make the charge transfer through the surface

(via diffusion in occluded solution) easier with increasing surface strain. As a result, corrosion resistance of bent NiTi wires decreases with increasing surface strain (decreasing bending radius). As the fit of the equivalent circuit provided non-negligible values of the capacitance of oxide layer C_o , we may conclude (Ref 20) that there was a non-negligible presence of metal cation vacancies providing easier access of external ions to the material and, hence, negatively contributing to the corrosion process. More cationic vacancies in repassivated oxide layer cause higher capacitive response with the result that the layer is less resistant to dissolution and hence to crack propagation (Ref 21). This could possibly be also related to the subsurface NiTi layer which transforms to martensite upon bending and hence become “more open for the external ions.”

The overall changes in impedance observed in the Nyquist plot (Fig. 14a) are thus due to: (i) diffusion in cracked oxide layer and (ii) anodic reaction in the subsurface martensitically transformed layer, the role of which increases with decreasing bending radius. Significant change in impedance observed between samples L3 and L4 might be caused by higher stress due to straining the surface layer beyond the plateau range in case of L4 (Fig. 2). The phase shifts at low frequencies (see Bode plot in Fig. 14b) are due to the heterogeneity of the cracked surface and easier diffusion in it.

It is essential that, compared to the Potentiodynamic Polarization test most frequently used in NiTi corrosion studies in the literature, the surface oxide layer is only very slightly and reversibly polarized by the small AC amplitudes applied in the EIS measurement. The surface is thus exposed to similar conditions as the surfaces of NiTi implants in human body. Out of the three electrochemical methods employed, the EIS method thus seems to be the most appropriate one for the characterization of the effect of the degree of cracking within the oxide layers. The results of EIS and polarization tests are complementary. While the EIS test is more suitable for characterization of the electrochemical properties of the cracked oxide layers and better respects the nature of the NiTi corrosion process in the body, the potentiodynamic polarization test accelerates the corrosion processes and provides clear information on the corrosion resistance of the bent superelastic NiTi wires.

6. Conclusions

Electrochemical corrosion studies were carried out on straight and bent medical grade superelastic NiTi wires. Cracks within the surface oxide and NiTi matrix introduced by bending the wires were observed by FIB–SEM and TEM methods. It was found that density and width of the surface oxide cracks dramatically increase with decreasing bending radius and that the surface oxide cracks introduced by bending cross over into the NiTi matrix.

The results of all three electrochemical tests consistently show that corrosion properties of the bent NiTi wires with cracked oxide layers (static load keeps the cracks opened) are inferior compared to the corrosion properties of the straight wires (virgin uncracked oxide). Microcracks in the cracked oxide layer are held responsible for the observed degradation of the corrosion behavior of the bent NiTi wires. A mechanism by which the presence of oxide cracks affects the corrosion behavior in electrochemical tests is proposed, modeled, and discussed.

Out of the three methods employed, the Electrochemical Impedance Spectroscopy seems to be the most appropriate test

for the electrochemical characterization of the cracked oxide layers since the impedance curves of differently bent NiTi wires can be associated with the state of the surface cracking and since the NiTi wires are exposed in the EIS tests to similar conditions as the surfaces of NiTi implants in a human body. On the other hand, the potentiodynamic polarization test accelerates the corrosion processes and provides clear information on the corrosion resistance of the bent superelastic NiTi wires.

Acknowledgment

This research has been supported by the 7RPEU project SMARTNETS (FP7-NMP2010-SMALL-262806) and by the projects P107/12/0800 and P108-12-P111 of the Grant Agency of the Czech Republic. The authors would like to express special thanks to prof. Jan Van Humbeeck from MTM Department KU Leuven for consultancy and providing access to the FEI SEM facility as well as to Neil Othen from GATAN for the same regarding the tensile stage Microtest 2000EWN.

References

1. K. Volenec, On the use of Nitinol in corrosive environments in clinical practice, Proceedings of SMST 2013
2. K. Hírmanová, J. Pilch, J. Racek, L. Heller, P. Šittner, L. Recman, M. Petrevec, P. Sedlák, Physical simulation of the random failure of implanted braided niti stents, *J. Eng. Mater. Perform.* this issue
3. S.A. Shabalovskaya, G.C. Rondelli, A.L. Undisz, J.W. Anderegg, T.D. Burleigh, and M.E. Rettenmayr, The electrochemical characteristics of native Nitinol surfaces, *Biomaterials*, 2009, **30**, p 3662–3671
4. C. Trepanier, A. R. Pelton, Effect of strain on the corrosion resistance of nitinol and stainless steel in simulated physiological environment, Proceedings of SMST 2003
5. T. Kanemura, K. Yokoyama, and J. Sakai, Effects of acid type on corrosion and fracture behavior of Ni–Ti superelastic alloy under sustained tensile load in physiological saline solution containing hydrogen peroxide, *Corros Sci.*, 2008, **50**, p 2785–2795
6. M. Rahim, J. Frenzel, M. Frotscher, J. Pftzing-Micklich, R. Steegmuller, M. Wohlschlogel, H. Mughrabi, and G. Eggeler, Impurity levels and fatigue lives of pseudoelastic NiTi shape memory alloys, *Acta Mater.*, 2013, **61**, p 3667–3686
7. P. Sedlak, M. Frost, B. Benesova, P. Sittner, and T. Ben, Zineb, thermomechanical model for NiTi based shape memory alloys including R-phase and material anisotropy under multi-axial loadings, *Int. J. Plast.*, 2012, **39**, p 132–151
8. G.S. Firstov, R.G. Vitchev, H. Kumar, B. Blanpain, and J. Van Humbeeck, Surface oxidation of NiTi shape memory alloy, *Biomaterials*, 2002, **23**, p 4863–4871
9. P. Filip, J. Lausmaa, J. Musialek, and K. Mazanec, Structure and surface of TiNi human implants, *Biomaterials*, 2001, **22**, p 2131–2138
10. H. Tian, D. Schryvers, S. Shabalovskaya, and J. Van Humbeeck, Microstructure of surface and subsurface layers of a Ni–Ti shape memory microwire, *Microsc. Microanal.*, 2009, **15**, p 62–70
11. R. Hang, S. Ma, V. Ji, and P.K. Chu, Corrosion behavior of NiTi alloy in fetal bovine serum, *Electrochim Acta*, 2010, **55**, p 5551–5560
12. X. Li, J. Wang, E. Han, and W. Ke, Influence of fluoride and chloride on corrosion behavior of NiTi orthodontic wires, *Acta Biomater.*, 2007, **3**, p 807–815
13. A.S. Bondarenko, Analysis of large experimental datasets in electrochemical impedance spectroscopy, *Anal Chimica Acta*, 2012, **743**, p 41–50
14. I. Martínez and C. Andrade, Application of EIS to cathodically protected steel: tests in sodium chloride solution and in chloride contaminated concrete, *Corrosion Science*, 2008, **50**, p 2948–2958
15. P. Sedlák, M. Frost, K. Hírmanová, L. Heller, P. Šittner, Simulations of mechanical response of superelastic NiTi helical spring and its relation to fatigue resistance, *J. Mater. Eng. Perform.*, in this issue
16. K. Yokoyama, T. Eguchi, K. Asaoka, and M. Nagumo, Effect of constituent phase of Ni–Ti shape memory alloy on susceptibility to hydrogen embrittlement, *Mater. Sci. Eng. A*, 2004, **374**, p 177–183
17. K. Asaoka, K. Yokoyama, and M. Nagumo, Hydrogen embrittlement of nickel-titanium alloy in biological environment, *Metall. Mater. Trans.*, 2002, **33A**, p 495–501
18. J. Ai, Y. Chen, M. Urquidi-Macdonald, and D.D. Macdonald, Electrochemical impedance spectroscopic study of passive zirconium, *J. Nucl. Mater.*, 2008, **379**, p 162–168
19. D.D. Macdonald, The history of the point defect model for the passive state: a brief review of film growth aspects, *Electrochim. Acta*, 2011, **56**, p 1761–1772
20. G. Bellanger, Corrosion induced by low-energy radionuclides, 2004, p. 151–160
21. J. Wang, N. Li, G. Rao, E. Han, and W. Ke, Stress corrosion cracking of NiTi in artificial saliva, *Dent. Mater.*, 2007, **23**, p 133–137
22. D. Yang, Ch. Liu, X. Liu, M. Qi, and G. Lin, EIS diagnosis on the corrosion behavior of TiN coated NiTi surgical alloy, *Curr. Appl. Phys.*, 2005, **5**, p 417–422